

Spin Chemical Approach towards Long-Lived Charge-Separated States Generated by Photoinduced Intramolecular Electron Transfer in a Donor–Bridge–Acceptor System

Yukie Mori, Yoshio Sakaguchi, and Hisaharu Hayashi*

Molecular Photochemistry Laboratory, RIKEN (The Institute of Physical and Chemical Research), Hirosawa, Wako, Saitama 351-0198

(Received September 1, 2000)

Photo-induced intramolecular electron transfer (ET) and subsequent back ET have been studied for phenothiazine–bridge–pyromellitdiimide (D–B–A) and phenothiazine–bridge–pyromellitdiimide–nitroxide radical (D–B–A–R•) in various solvents by nano-second transient absorption spectroscopy. Upon excitation of the phenothiazine (D) moiety in these compounds, ET from $^1D^*$ to A took place at a rate of ca. 5×10^9 s^{-1} to give charge-separated (CS) states, $^1[D^{\bullet+}–B–A^{\bullet-}]$ or $^2[D^{\bullet+}–B–A^{\bullet-}–R\bullet]$, in high quantum yields. The decay dynamics of the CS states was determined by the interplay between the spin conversion and the back ET to the ground state. The efficiency of the interconversion between states with different spin multiplicities was strongly affected by the presence of R• and external magnetic fields. A faster spin conversion of $[D^{\bullet+}–B–A^{\bullet-}–R\bullet]$ resulted in a slower initial decay of the CS state generated from the excited singlet state of D compared with $[D^{\bullet+}–B–A^{\bullet-}]$. Such a spin effect manifested most markedly in dioxane. On the other hand, the back ET rate (k_{BET}) varied by more than two orders of magnitude with the solvent polarity. In dimethyl sulfoxide, the back ET was predicted to be almost barrierless, $k_{BET} \geq 10^9$ s^{-1}, while in benzene, this process fell in the inverted region, $k_{BET} = 6.5 \times 10^6$ s^{-1}.

Photo-induced electron transfer (ET) reactions have been extensively investigated for a variety of donor(D)–acceptor(A) dyads as well as D–D′–A or D–A–A′ triads. These studies have been aimed at mimicking the highly efficient charge separation in the natural photosynthetic reaction center (RC).[1–3] Many efforts have also been made to elucidate the mechanisms, dynamics, and factors governing the rates for ET reactions in chemically and biologically important systems.[4] In most of the photo-induced ET systems reported so far, including the RCs, the excited singlet states of the light-absorbers undergo charge separation to give the radical ion pair states (RIPs); therefore, the fast spin-allowed charge recombination to give the ground states inevitably shortens the lifetimes of the RIP intermediates. On the other hand, for the modified RCs[5] and synthetic model compounds,[6] the long-lived triplet RIPs were characterized by time-resolved EPR studies. The charge recombination rates of such long-lived RIPs could be reduced not only by the large separation distance, but also by the spin forbiddeness for the triplet states. Thus, spin evolution can play an important role in a sequence of ET processes, such as charge separation, charge shift, and charge recombination. For typical RIPs consisting of two organic ion radicals, spin conversion from the singlet to the triplet states occurs at a rate of, at most, $\sim 10^8$ s^{-1}, while ET reactions can take place much faster.

Recently, we have found that spin conversion processes in RIPs and biradicals were accelerated by the presence of an unreactive radical in the proximity of one of the component radicals and that the spin dynamics of such three-spin systems was modulated by an external magnetic field.[7,8] The variations in the spin dynamics of the intermediates were well reflected in their lifetimes and/or the product yields under appropriate conditions. These results prompted us to study the photoinduced ET of a donor (D)–bridge (B)–acceptor (A)–radical (R•) system toward the formation of long-lived charge-separated (CS) states by a new approach based on spin dynamics. Elucidation of the role of an additional radical center is also important in the field of spin chemistry, because such an unreactive radical center has been utilized as an "observer" of the spin dynamics of the radical pair (RP) in EPR studies,[9] while an ability as a "catalyst" for the spin conversion processes of RP has been proposed.[10,11]

In the present study, we have investigated the reaction pathways and dynamics of photo-induced charge separation in D–B–A–R• and of the charge recombination in the resultant CS state by means of a nano-second laser flash technique in solvents of various polarity. Chart 1 shows the compounds (**1**–**5**) studied in this work. Here, we used phenothiazine and 1,2:4,5-pyromellitdiimide as D and A, respectively. The bridging part was a semi-rigid biphenyl-4,4′-bis(methylene) unit. The stable radical R• used was 2,2,6,6-tetramethylpiperidin-1-oxyl (TEMPO), which was directly linked to A (compound **3** in Chart 1). To clarify the effect of R• on the decay dynamics of the CS state, we also examined the corresponding two-spin system ($D^{\bullet+}–B–A^{\bullet-}$), which was generated upon the excita-

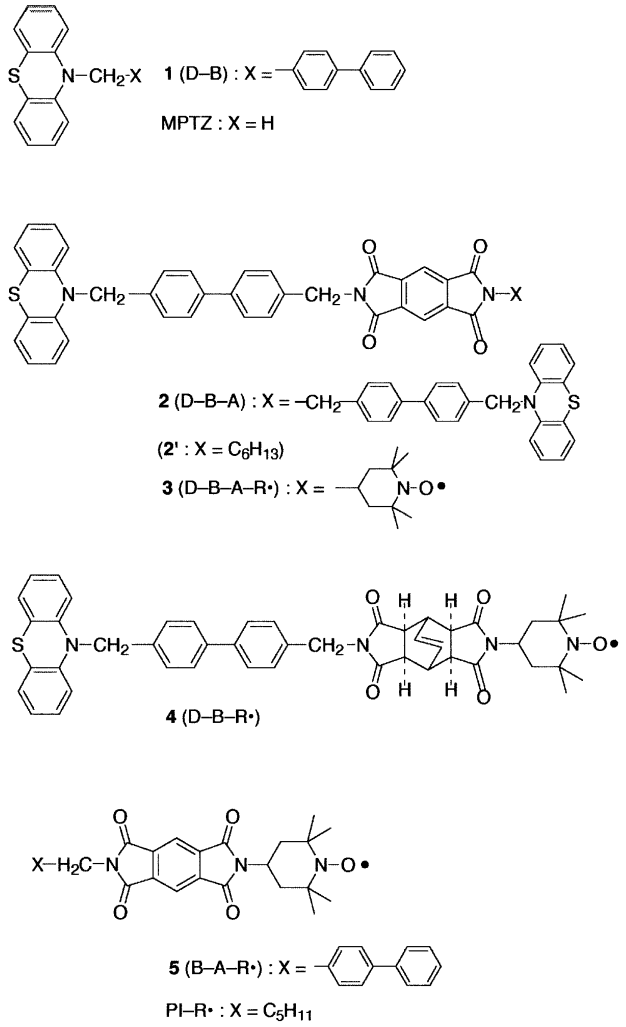

Chart 1.

tion of **2**. The major photochemical process was ET from the lowest singlet excited state of the donor part ($^1D^*$) to A for both **2** and **3**. The presence of R• accelerated the conversion from the initially populated doublet spin states to the chemically inactive quartet ones, retarding the decay of the CS state through back ET. The solvent polarity was also found to be an important factor in determining the lifetimes of the CS states derived from **2** and **3** through a large variation in the spin-allowed back ET rate.

Results

1. Photo-induced Charge Separation. To investigate the intramolecular quenching of $^1D^*$ by A, we measured the fluorescence spectra of D–B (**1**), D–B–A (**2**), and D–B–A–R• (**3**). Compound **1** showed broad fluorescence emission with an ill-resolved vibronic structure around 440 nm in both polar and non-polar solvents at 293 K. The spectral shape of **1** was quite similar to that of the fluorescence (λ_{max} = 447 nm in MeCN) of 10-methylphenothiazine (MPTZ). The fluorescence quantum yield of **1** in MeCN was ca. 0.01, and the ratio to that of MPTZ was 0.96. These results indicate that the (biphenyl-4-yl)methyl substituent at the 10-position gives no significant perturbation to the electronic structure of the S_1 state of the phenothiazine chromophore. The D–B–A and D–B–A–R• compounds, **2** and **3** respectively, exhibited fluorescence spectra which were similar to each other, but their intensities were reduced to about one-tenth or less that of **1**, as shown in Table 1. Because asymmetric diimide **2′** (Chart 1) could not be obtained in a pure state (see Experimental), symmetric diimide **2** was used as the D–B–A compound. The similarity in the fluorescence spectral shape among **1**–**3** indicated that the two D–B parts in **2** showed no significant interaction in the S_1 state. The fluorescence quenching observed for **2** and **3** suggested that intramolecular ET took place from $^1D^*$ to A to give the CS state, which was confirmed by the nano-second laser flash photolysis.

Figure 1 shows the transient absorption spectra for a benzene solution of **3** recorded at various delay times after excitation with a 355 nm laser pulse. The intense peaks at 720 and 660 nm are assigned to absorption due to the radical anion of the 1,2 : 4,5-pyromellitdiimide moiety ($A^{\bullet-}$),[7b] while the weaker broad band around 530 nm is assigned to the radical cation of the phenothiazine part ($D^{\bullet+}$).[12,13] These absorption bands appeared instantaneously after excitation and decayed to the zero level in ca. 2 μs with no change in the spectral shape. Upon the excitation of **2** in toluene, a quite similar transient spectrum was observed. The transient spectrum for **1** showed a broad band at 470 nm, which was assigned to the absorption due to the lowest triplet excited (T_1) state of the phenothiazine part ($^3D^*$) from the reported T–T absorption spectrum of MPTZ (λ_{max} = 465 nm, $\varepsilon_{max} = 2.3 \times 10^4$ M^{-1} cm^{-1}).[12] In the transient spectra for **2** and **3**, no absorption band assignable to the T–T

Table 1. Integrated Fluorescence Intensities (I_{FL})[a] of **2**–**4** Relative to That of **1** and the ET Rate (k_{ET}) in Various Solvents at 293 K on Excitation at 355 nm

Solvent	I_{FL}(**2**)/I_{FL}(**1**)	k_{ET} /10^9 s^{-1} [b]	I_{FL}(**3**)/I_{FL}(**1**)	I_{FL}(**4**)/I_{FL}(**1**)
Benzene	0.105	4.3	0.092	0.86
Dioxane	0.096	4.7	0.072	—[c]
THF	0.097	4.7	0.074	—[c]

a) Integrated over 390–600 nm. b) Calculated by Eq. 3. c) Not measured.

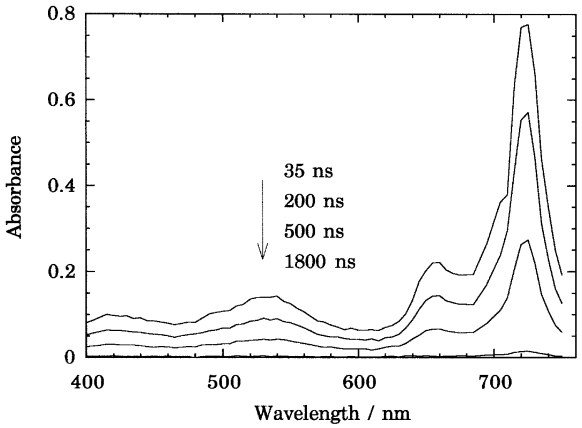

Fig. 1. Transient absorption spectra of **3** in benzene at various delay times after excitation.

absorption was observed.

As can be seen in Table 1, the fluorescence yield of **3** was somewhat lower than that of **2** in each solvent, suggesting that there should be another process responsible for the fluorescence quenching of **3**. It has been reported that nitroxide radicals, such as TEMPO, can quench the excited singlet states through energy transfer and/or enhanced intersystem crossing (ISC).[14] To examine the possibility of the fluorescence quenching by R• in **3**, we also measured the relative fluorescence intensity for D–B–R• model compound **4**,[15] in which the diimide moiety does not act as an electron acceptor. The fluorescence intensity of **4** was somewhat lower than that of **1**. This partial quenching is likely to be due to excitation energy transfer via the Förster mechanism, because the fluorescence spectrum of ^{1}D* is largely overlapped with the absorption band of TEMPO (λ_{max} = 470 nm in benzene). These results indicated that the ^{1}D* in **3** is quenched through energy transfer to R• as well as ET. The reaction pathways for **2** and **3** are represented in Schemes 1a and 1b, respectively.

2. Effects of Spin Multiplicity and Magnetic Fields on Decay Dynamics of the CS States in Dioxane. To investigate the effects of the presence of R• on the decay dynamics of the CS states, we measured the time profiles of the transient absorbance, $A(t)$ curves, due to the CS states by irradiating of **2** and **3** with a 355-nm laser pulse in several solvents. Although the decay dynamics of the CS states derived from **2** and **3** were different from each other in either solvent, the most prominent spin effect was observed in dioxane. Figure 2(a) shows the $A(t)$ curves monitored at 650 nm for **3** in dioxane under various magnetic fields (B's). The $A(t)$ curve under zero field can be fitted to a mono-exponential decay with a rate constant of 6.87×10^6 s^{-1}. Because this observed rate constant corresponds to a quarter of the k_{BET} value (See Section 2a in Discussion), k_{BET} in dioxane was determined to be 2.74×10^7 s^{-1}.

Figure 3a shows the $A(t)$ curves monitored at 715 nm for **2** in dioxane under conditions similar to those for Fig. 2a .The $A(t)$ curve for **2** under zero field was strongly biphasic. The decay of

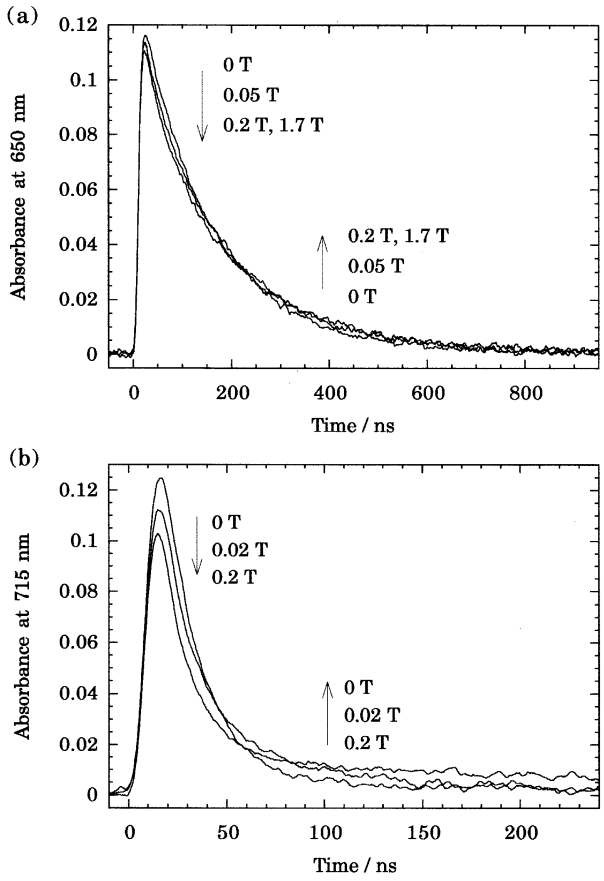

Fig. 2. $A(t)$ curves monitored at 650 nm for **3** on excitation at 355 nm under various magnetic fields (a) in dioxane and (b) in pentyl acetate.

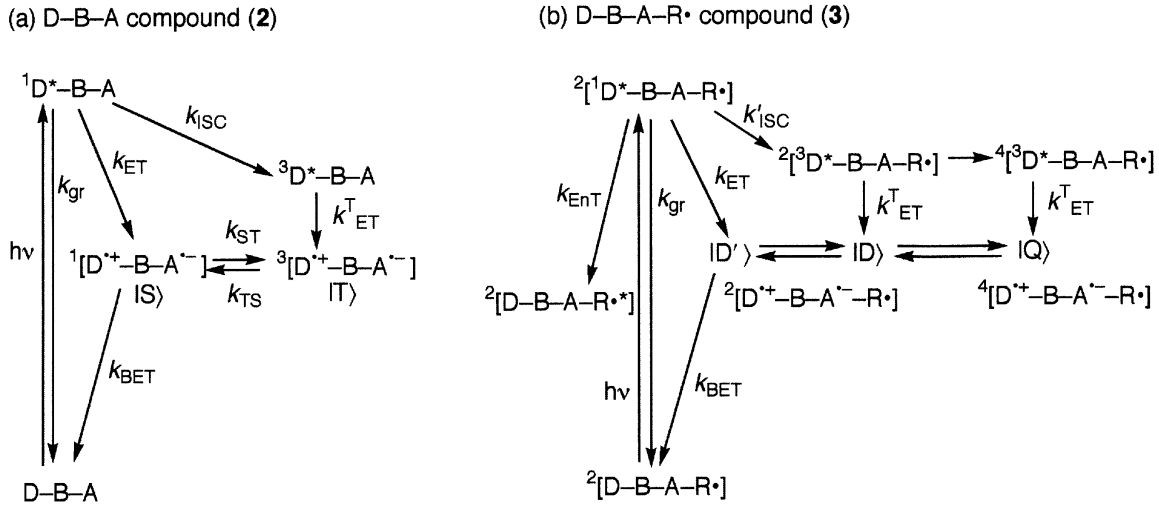

Scheme 1. Reaction pathways for (a) **2** and (b) **3** on excitation of the phenothiazine chromophore. The k's denote the rate constants for the processes: k_{gr}, radiative and non-radiative decay to the ground state; k_{ISC} (k'_{ISC}), intersystem crossing from ^{1}D* to ^{3}D*; k_{EnT}, excitation energy transfer from ^{1}D* to R•; k_{ET}, ET from ^{1}D* to A; k^T_{ET}, ET from ^{3}D* to A; k_{ST}, spin conversion from ^{1}CS to ^{3}CS; k_{TS}, spin conversion from ^{3}CS to ^{1}CS; k_{BET}, spin-allowed back ET reaction from A$^{\bullet-}$ to D$^{\bullet+}$ within the CS state.

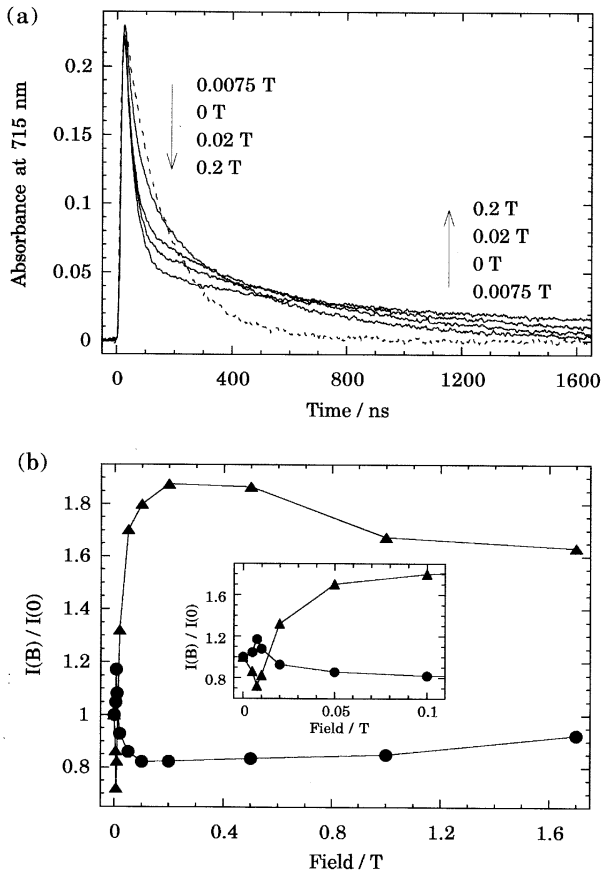

Fig. 3. (a) $A(t)$ curves monitored at 715 nm for **2** on excitation at 355 nm under various magnetic fields in dioxane. The broken line shows the normalized $A(t)$ curve for **3** in dioxane under zero field. (b) Ratios of the integrated absorbance in the presence and absence of each magnetic field in the time windows of 10–300 ns (circle) and 450–3350 ns (triangle) after excitation.

the shorter-lived component was much faster than that of the CS state derived from **3**, [D$^{\bullet+}$–B–A$^{\bullet-}$–R•] (broken line in Fig. 3a). This $A(t)$ curve for **2** can be fitted to a double exponential function with rate constants of 3.27×10^7 s^{-1} (k_1) and 1.72×10^6 s^{-1} (k_2). As shown in Scheme 1a, ^{1}[D$^{\bullet+}$–B–A$^{\bullet-}$] (|S⟩) decays through the back ET and spin conversion to ^{3}[D$^{\bullet+}$–B–A$^{\bullet-}$] (|T⟩). Under zero field, each of the three sublevels of |T⟩ is converted to |S⟩ at a rate of k_{TS}, and the reverse conversion from |T⟩ to |S⟩ takes place at a rate of $k_{ST} = 3k_{TS}$. Under such conditions, k_1 and k_2 are related to k_{TS} and k_{BET} by

$$k_{1,2} = 1/2[4k_{ISC} + k_{BET} \pm (16{k_{TS}}^2 + 4k_{TS}k_{BET} + {k_{BET}}^2)^{1/2}]. \quad (1)$$

The solution of Eq. 1 gave k_{TS} and k_{BET} values of 2.2×10^6 and 2.56×10^7 s^{-1}, respectively. The obtained k_{BET} value is in fairly good agreement with the value (2.74×10^7 s^{-1}) determined for [D$^{\bullet+}$–B–A$^{\bullet-}$–R•].

Due to the presence of R•, MFEs on the decay of [D$^{\bullet+}$–B–A$^{\bullet-}$–R•] were also different from those of [D$^{\bullet+}$–B–A$^{\bullet-}$]. As can be seen in Fig. 2a, the $A(t)$ curves observed for **3** under $B \geq 0.05$ T exhibited a small deviation from a mono-exponential decay. At an early stage ($0 < t < 200$ ns), the $A(t)$ value decreased slightly with increasing B, while at later times ($t > 200$ ns) it marginally increased with increasing B. More distinctive MFEs on the decay of [D$^{\bullet+}$–B–A$^{\bullet-}$–R•] were observed in pentyl acetate (PenOAc), as shown in Fig. 2b. In this solvent, the $A(t)$ curve under zero field consisted of a major fast decaying component and a minor slow decaying one. The former component decayed much faster than the $A(t)$ curve observed in dioxane. With increasing B, the $A(t)$ value at an early time region ($t < 50$ ns) decreased while that at later times ($t > 80$ ns) increased. This tendency of the MFEs observed in PenOAc was the same as that observed in dioxane (Fig. 2a), but the magnitudes of the MFEs in PenOAc were larger than those in dioxane. The $A(t)$ curves in PenOAc under different B's intersected at a much earlier time than those in dioxane. The magnetically induced changes in PenOAc were monotonous from 0 to 0.2 T, but no further change was observed in the field range of 0.2–1.7 T.

The decay of [D$^{\bullet+}$–B–A$^{\bullet-}$] in dioxane exhibited complicated MFEs in the field range of 0–0.2 T, as shown in Fig. 3a. The $A(t)$ curves under different B's intersect at 400–600 ns, indicating that the observed MFEs before this intersection have an opposite tendency to those after the intersection. To represent this peculiar feature of MFEs, we integrated the $A(t)$ curves in time windows of 10–300 and 450–3350 ns and plotted the relative integration values, $I_{10}(B)/I_{10}(0)$ and $I_{450}(B)/I_{450}(0)$, against B in Fig. 3b. As shown in this figure, the $I_{10}(B)$ value steeply increased with increasing B from 0 to 7.5 mT, decreased from 7.5 mT to 0.2 T, and finally slightly decreased from 0.2 to 1.7 T. On the other hand, the $I_{450}(B)$ value showed opposite B-dependence to the $I_{10}(B)$ one. Similar biphasic decay kinetics and MFEs were reported for the CS states derived from fixed-distance triads consisting of porphyrins and an electron acceptor in THF solution.[16] These MFEs can be explained by combining the level-crossing mechanism (LCM)[17] and the relaxation mechanism (RM)[18] for singlet-born radical pairs, as discussed later (See Section 2c in Discussion).

3. Solvent Effects on the Decay of the CS States. To investigate solvent effects on the k_{BET} value, we measured the $A(t)$ curves for **3** in solvents of different polarity. Figure 4 shows the normalized $A(t)$ curves observed for **3** under zero field. The lifetime of [D$^{\bullet+}$–B–A$^{\bullet-}$–R•] decreased along with an increase in the solvent polarity. The $A(t)$ curves observed in toluene and benzene under zero field exponentially decayed with rate constants smaller than that observed in dioxane. The obtained k_{BET} values are listed in Table 2. In the presence of B's below 1.7 T, the $A(t)$ curves in toluene and benzene exhibited the same type of small deviation from a mono-exponential decay as in dioxane.

In THF, MeCN, and DMSO,[19] the $A(t)$ curves showed a biphasic nature under zero field, and the initial decay was faster than that observed in PenOAc. No difference in the initial decay rate was detected among the THF, MeCN, and DMSO solutions. However, when each of the sample solutions with the same optical density at 355 nm was excited under the same conditions, the maximal $A(t)$ value, A_{max}, at 715 nm in MeCN

or DMSO was lower than that observed in THF (in Fig. 4, each of the $A(t)$ curves was normalized relative to its A_{max}). This difference in the A_{max} value suggests that the decay through back ET of ^{2}[D$^{\bullet+}$–B–A$^{\bullet-}$–R•] in MeCN and DMSO should be faster than that in THF. Thus, the k_{BET} value was found to increase in the order benzene < toluene < dioxane << PenOAc < THF < MeCN ~ DMSO, as the solvent polarity increases.

The decay dynamics of [D$^{\bullet+}$–B–A$^{\bullet-}$] also depended on the solvent polarity. Figure 5a shows the $A(t)$ curves upon the excitation of **2** in toluene under various B's. Under zero field, the decay rate was larger and smaller than that of [D$^{\bullet+}$–B–A$^{\bullet-}$–R•] (broken line in Fig. 5a) in early ($t \leq 400$ ns) and later ($t \geq 600$ ns) time regions, respectively. This feature is similar to that observed in dioxane (Fig. 3a), although the overall decay of [D$^{\bullet+}$–B–A$^{\bullet-}$] in toluene was much slower than that observed in dioxane. The $A(t)$ curves observed in THF under zero field also showed biphasic decay, as shown in Fig. 5b. In DMSO, the initial decay part was too fast to observe with our nano-second apparatus. Thus, the decay rate at early times ($t < 100$ ns) increased in the order toluene < dioxane < THF < DMSO. The acceleration of the initial decay in polar solvents reflects the increase in the k_{BET} value with increasing solvent polarity, as was the case for [D$^{\bullet+}$–B–A$^{\bullet-}$–R•].

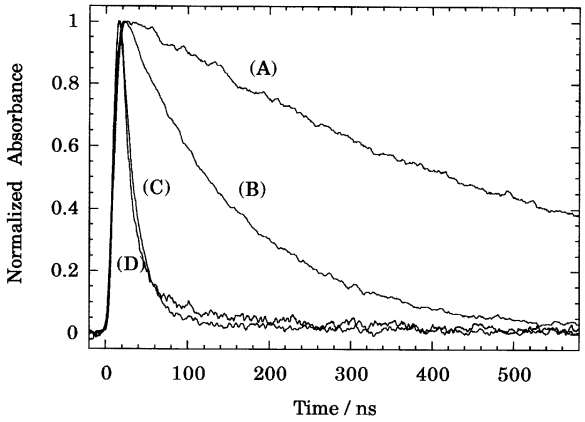

Fig. 4. $A(t)$ curves for **3** under zero field in (A) toluene, (B) dioxane, (C) pentyl acetate, and (D) THF. The monitored wavelength is 650 nm for (A) and (B) or 715 nm for (C) and (D). Each of the $A(t)$ curves are normalized with respect to the maximal value.

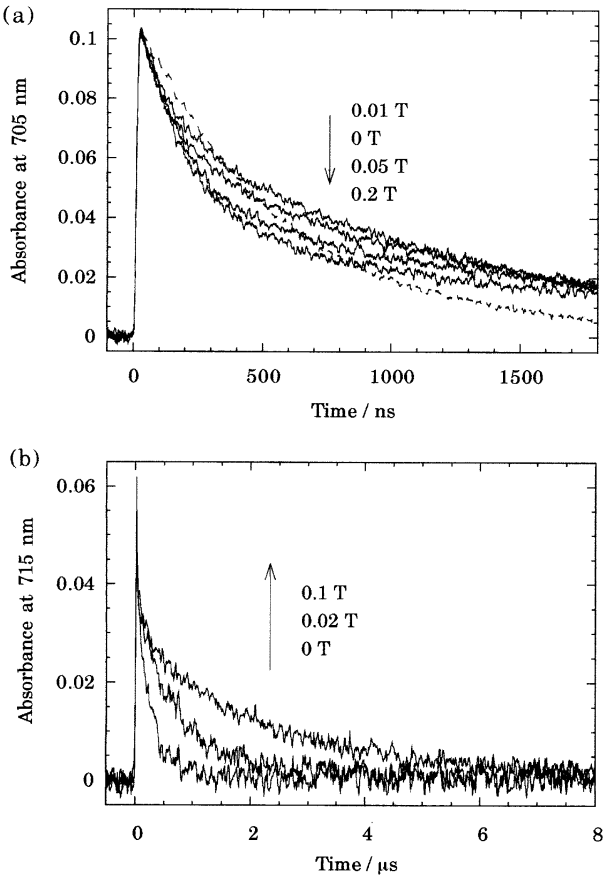

Fig. 5. $A(t)$ curves for **2** under various magnetic fields in (a) toluene and (b) THF. The broken line shows the $A_{650}(t)$ curve for **3** in toluene under zero field.

As can be seen in Fig. 5a, the $A(t)$ value in the monitored time window ($t < 1800$ ns) for the toluene solution of **2** decreased from 0 to 0.01 T, increased from 0.01 to 0.35 T, and slightly decreased from 0.35 to 1.7 T. This B-dependence is quite similar to that observed for the $A(t)$ curves in the time window of 10–300 ns in dioxane (Fig. 3b), and explained by the same mechanisms as the MFEs observed in dioxane. On the other hand, a different type of MFE was observed in THF. As shown in Fig. 5b, the decay rate in microsecond time region markedly decreased with an increase in B from 0 to 0.1 T. With a further increase in B, although no change in the $A(t)$ curves

Table 2. Properties of Solvents,[a] Free Energy Change (ΔG_{BET}), Total Reorganization Energy (λ), and Rate Constant (k_{BET}) of Back ET for the CS State Derived from **3** at 293 K

Solvent	ε_r	$1/n^2 - 1/\varepsilon_r$	ΔG_{BET}[b]/eV	λ[b]/eV	k_{BET}/s^{-1}
Benzene	2.2825	0.0057	(−2.3)[c]	(0.7)[d]	6.5×10^6
Toluene	2.379	0.0259	N.A.[e]	N.A.[e]	7.4×10^6
Dioxane	2.2189	0.0436	(−2.15)[c]	(0.85)[f]	2.7×10^7 [2.6×10^7][g]
Pentyl acetate	4.79	0.2994	(−2.0)	(1.1)	$\geq 10^8$
THF	7.52	0.3720	−1.81	1.3	$\geq 10^8$
DMSO	47.24	0.4358	−1.51	1.5	$\geq 10^9$
MeCN	36.64	0.5262	−1.52	1.7	$\geq 10^9$

a) Ref. 40. b) Values in parentheses are approximate. c) See text. d) λ_{sol} is assumed to be 0.4 eV. e) Not available. f) λ_{sol} is assumed to be 0.55 eV. g) Obtained for **2**.

was observed from 0.1 to 0.5 T, the decay became slightly faster from 0.5 to 1.7 T. In DMSO, the $A(t)$ curve showed MFEs similar to those observed in THF. These MFEs can be explained by the RM for triplet-born radical pairs. This result indicated that ^{3}D*–B–A also underwent intramolecular ET to give ^{3}[D$^{\bullet+}$–B–A$^{\bullet-}$] in polar solvents, such as THF and DMSO. No MFE due to the LCM was observed in THF or DMSO.

Discussion

1. Photo-induced Charge Separation. (a) Energy Levels of the CS States. As demonstrated by fluorescence and transient absorption studies, the intramolecular ET from ^{1}D* to A in **2** and **3** took place sufficiently fast to compete with ISC to ^{3}D* in various solvents. The free-energy change (ΔG_{ET}) accompanying this ET process can be estimated by Eq. 2.[20]

$$\Delta G_{ET} = (E^{D}_{OX} - E^{A}_{RED})_{MeCN} - e^2/(4\pi\varepsilon_0\varepsilon_r R) + e^2/(8\pi\varepsilon_0)(1/r_D + 1/r_A)(1/\varepsilon_r - 1/\varepsilon_{MeCN}) - E_S \quad (2a)$$

$$= -\Delta G_{BET} - E_S \quad (2b)$$

Here, E^{D}_{OX} and E^{A}_{RED} are the oxidation potential of D and the reduction potential of A, respectively, measured in MeCN. Because the solubility in MeCN of **2** and **3** was too low for electrochemical studies, E^{D}_{OX} = +0.345 V and E^{A}_{RED} = –1.21 V (vs. ferrocene) were used, which were measured for **1** and **5**, respectively. ε_r and ε_{MeCN} are the relative permittivities of the solvent used for the ET reaction and of MeCN, respectively. The ionic radii of D$^{\bullet+}$ and A$^{\bullet-}$ are denoted by r_D and r_A, respectively, where $r_D = r_A$ = 3.7 Å were used. R is the center-to-center distance between D$^+$ and A$^-$, which was assumed to be 12 Å on the basis of the PM3[21]-optimized structure for one of the stable conformers in the neutral ground state.[22] As the singlet excitation energy of D (E_S), the reported value for MPTZ (2.9 eV[23]) was used. ΔG_{BET} represents the free-energy change accompanying back ET from A$^{\bullet-}$ to D$^{\bullet+}$ within the CS state to give the ground state. The ΔG_{ET} values are estimated to be –0.28, –0.24, –1.09, –1.39, and –1.38 eV in benzene, dioxane, THF, DMSO, and MeCN, respectively. However, Eq. 2 probably underestimates the driving force for charge separation in benzene and dioxane.

According to Warman et al.,[24] the energy levels of the CS states for donor–acceptor compounds separated by σ-bonds were lower by 0.4 and 0.56 eV in benzene and dioxane, respectively, than in saturated hydrocarbon solvents such as decalin. They attributed this stabilization to quadrupolar interactions between the solvent molecules and charged centers. Although the quite low solubility of **2** and **3** to saturated hydrocarbons precluded us from investigating in such solvents, the CS states derived from these compounds are likely to be stabilized in benzene and dioxane by the same type of solvent–solute interactions. In addition, the R value may be smaller than that estimated for the parent neutral species to cause a larger Coulombic attraction between D$^{\bullet+}$ and A$^{\bullet-}$. With respect to this point, Shephard and Paddon-Row predicted based on the *ab initio* calculations that the molecular structures can be significantly deformed upon the charge-separation process in D–B–A systems whose structures are believed to be rather rigid.[25] Although their calculations were carried out for ET reactions in the gas phase, such structural deformation may be induced to some extent in solvents with low dielectric constants. Thus, the intramolecular ET from ^{1}D* to A is exothermic by at least 0.28 eV or more in all of the solvents examined.

The unquenched ^{1}D* mainly undergoes ISC to the T_1 state, because the quantum yield of formation of the T_1 state was reported to be close to unity for MPTZ.[12] A possible explanation for the lack of the T–T absorption band in the transient spectra of **2** and **3** is that ^{3}D* may rapidly decay through ET. The free-energy change of ET from ^{3}D* to A in polar solvents can be estimated from Eq. 2 by using the triplet excitation energy (E_T) reported for MPTZ (2.64 eV[12]) instead of E_S. The calculated values are –0.83, –1.13, and –1.12 eV in THF, DMSO, and MeCN, respectively, suggesting that ET in the triplet manifold can take place rapidly in these solvents.

(b) ET Rate Constants. The experimental rate constant (k_{ET}) of ET from ^{1}D* to A for **2** was obtained from the relative intensities of the fluorescence by

$$k_{ET} = \tau_0(\mathbf{1})^{-1}[(I_{FL}(\mathbf{1})/I_{FL}(\mathbf{2})) - 1], \quad (3)$$

where $I_{FL}(\mathbf{1})$ and $I_{FL}(\mathbf{2})$ represent the integrated fluorescence intensities for **1** and **2**, respectively. $\tau_0(\mathbf{1})$ is the lifetime of the S_1 state of **1**, which is assumed to be the same as that of MPTZ (2 ns in ethyl acetate,[26] MeCN,[26] and MeCN–water[23]). As shown in Table 1, the k_{ET} values were similar to each other in benzene, dioxane, and THF.

According to the Marcus theory,[27] k_{ET} for nonadiabatic ET is expressed by

$$k_{ET} = 2\pi|V|^2(\pi/\lambda k_B T)^{1/2}\exp[-(\Delta G_{ET} + \lambda)^2/4\lambda k_B T], \quad (4)$$

where V is the matrix element of electronic coupling,[28] and λ is the total reorganization energy, which consists of the contributions from solvent mode (λ_{sol}) and internal vibrations (λ_{vib}). Although the exact value of ΔG_{ET} is unknown for each solvent, it probably decreases in the order of benzene > dioxane > THF. On the other hand, λ_{sol} increases in the order of benzene < dioxane < THF with an increase in polarity.[27] As a result, the Franck–Condon factors in Eq. 4 may be similar to each other for these solvents, which accounts for the small solvent dependence of k_{ET}. A similar insensitivity to the solvent polarity of the ET rate was reported for the photo-induced intramolecular charge separation in some D–B–A systems.[24]

(c) Efficiencies of the Charge Separation. Based on Scheme 1a, the quantum yields of formation of ^{1}[D$^{\bullet+}$–B–A$^{\bullet-}$] and ^{3}[D$^{\bullet+}$–B–A$^{\bullet-}$] from **2** are expressed by Eqs. 5a and 5b, respectively:

$$\Phi^{S}_{CS}(\mathbf{2}) = k_{ET}/(k_{gr} + k_{ISC} + k_{ET}) = k_{ET}/(\tau_0^{-1} + k_{ET}), \quad (5a)$$

$$\Phi^{T}_{CS}(\mathbf{2}) = k^{T}_{ET}/(\tau_T^{-1} + k^{T}_{ET}) \times k_{ISC}/(\tau_0^{-1} + k_{ET}) \le k_{ISC}/(\tau_0^{-1} + k_{ET}) \approx 1 - \Phi^{S}_{CS}(\mathbf{2}), \quad (5b)$$

where τ_0^{-1} and τ_T^{-1} are the decay rates of ^{1}D*–B–A and ^{3}D*–B–A to the ground state, respectively. With the k_{ET} values

listed in Table 1 and an assumption that τ_0^{-1} should be the same as that of MPTZ (5×10^8 s^{-1}), $\Phi_{CS}^{S}(\mathbf{2})$ was estimated to be 0.9 in benzene, dioxane, and THF. Because τ_T^{-1} ($\sim 10^5$ s^{-1})[32] is probably much lower than k_{ET}^{T}, the $\Phi_{CS}^{T}(\mathbf{2})$ value could be close to 1–$\Phi_{CS}^{S}(\mathbf{2})$, which equals to 0.1. This upper limit of $\Phi_{CS}^{T}(\mathbf{2})$ was still much smaller than $\Phi_{CS}^{S}(\mathbf{2})$.

In the case of **3**, the quantum yield of ET from ^{1}D* to A is represented by

$$\Phi_{CS}(\mathbf{3}) = k_{ET}/(k_{gr} + k'_{ISC} + k_{EnT} + k_{ET}) = k_{ET} \times \tau(\mathbf{3}), \qquad (6)$$

where $\tau(\mathbf{3})$ is the lifetime of ^{2}[^{1}D*–B–A–R•], which can be evaluated as $\tau_0 \times I_{FL}(\mathbf{3}) / I_{FL}(\mathbf{1})$. Assuming that the k_{ET} value of **3** is the same as that of **2** in each solvent, we obtained $\Phi_{CS}(\mathbf{3})$ values of 0.8, 0.7, and 0.7 in benzene, dioxane, and THF, respectively. Thus, the major process in the decay of ^{2}[^{1}D*–B–A–R•] was the ET reaction with minor contribution from the energy transfer. This is consistent with the result that the fluorescence quenching for **4** was much less effective than that observed for **2** or **3**, as shown in Table 1. ET from ^{3}D* to A may also take place to give [D$^{•+}$–B–A$^{•-}$–R•] in either the doublet (|D⟩) or quartet (|Q⟩) sublevels depending on the total spin multiplicity of the precursor, ^{4,2}[^{3}D*–B–A–R•] (Scheme 1b). It was reported that the T_1 state of MPTZ was intermolecularly quenched by TEMPO through energy transfer (T–D quenching).[6] This quenching process requires a close contact of the triplet excited molecule and the radical.[33] In the case of **3**, the contribution of intramolecular T–D quenching is negligible because of the large separation distance between ^{3}D* and R•.

2. Spin Conversion Processes of the CS States. (a) Singlet–Triplet Conversion of [D$^{•+}$–B–A$^{•-}$]. First, we discuss the |S⟩ ↔ |T⟩ conversion of the two-spin intermediate, [D$^{•+}$–B–A$^{•-}$], and its B-dependence, which can be explained by the well-established mechanisms of MFEs for radical pairs. From an analysis of the $A(t)$ curve in dioxane under zero field, the |T⟩ → |S⟩ conversion rate (k_{TS}) of [D$^{•+}$–B–A$^{•-}$] was determined to be 2.2×10^6 s^{-1} (See Section 2 in Results). If the |S⟩ and |T⟩ states of [D$^{•+}$–B–A$^{•-}$] are degenerate, the HFC-induced |S⟩ ↔ |T⟩ conversion can occur at a rate of k_{HFC}, which is estimated to be 1.2×10^8 s^{-1} by Eq. 7;[34]

$$k_{HFC} = \pi g \beta B_{1/2}/h, \qquad (7a)$$

$$B_{1/2} = 2[|A_{HFC}(D^{•+})|^2 + |A_{HFC}(A^{•-})|^2] / [|A_{HFC}(D^{•+})| + |A_{HFC}(A^{•-})|]. \qquad (7b)$$

The effective HFC interactions for D$^{•+}$ and A$^{•-}$ were obtained by the relation $|A_{HFC}| = \Sigma_j[I_j(I_j + 1)a_j^2]^{1/2}$, where I_j and a_j are the spin quantum number and the isotropic HFC constant of the j-th nucleus. Here, the reported a_j values of MPTZ$^{•+}$ and the radical anion of *N*,*N*′-dihexyl-1,2 : 4,5-pyromellitdiimide[13,16] were used for D$^{•+}$ and A$^{•-}$, respectively. The observed k_{TS} value of [D$^{•+}$–B–A$^{•-}$] was much smaller than the calculated one. This reduction of the spin conversion rate is attributed to its exchange interaction, the absolute value ($|J|$) of which is larger than the magnitude of the effective HFC interactions.

The MFEs observed for the decay of [D$^{•+}$–B–A$^{•-}$] in dioxane (Fig. 3) and in toluene (Fig. 5a) can be explained by a combination of the LCM at $B \sim 7.5$ mT and the RM in the higher field region. As shown in Fig. 6a, the |S⟩ and |T⟩ states are energetically separated by $|2J| / g\beta$ (= ca. 7.5 mT) under zero field. Owing to this energy gap larger than the $B_{1/2}$ value (= 2.8 mT), the efficiency of the HFC-induced |S⟩ → |T⟩ conversion under zero field is lower than that of a biradical with $|2J| / g\beta = 0$ mT. As a result, most of [D$^{•+}$–B–A$^{•-}$] born in the |S⟩ state decays through back ET. With increasing B, the energy of the $|T_{+1}\rangle$ (or $|T_{-1}\rangle$) sublevel is raised (or lowered). Under $B = |2J| / g\beta$, where the energy level of $|T_{+1}\rangle$ (or $|T_{-1}\rangle$) matches that of |S⟩, HFC-induced |S⟩ → $|T_{+1}\rangle$ (or |S⟩ → $|T_{-1}\rangle$) conversion takes place in competition with back ET (Fig. 6b). Due to this enhancement of the |S⟩ → |T⟩ conversion, the apparent decay at the early stage ($t < 300$ ns) under $B = 7.5$ mT is retarded compared with that under zero field, as can be seen in Fig. 3a. Under fields higher than 7.5 mT, the $|T_{\pm1}\rangle$ sublevels decayed only through the $|T_{\pm1}\rangle$ → |S⟩ and $|T_{\pm1}\rangle$ → $|T_0\rangle$ relaxation, and the rates of these relaxation processes are much smaller than the |S⟩ ↔ $|T_0\rangle$ conversion rate and k_{BET} (Fig. 6c). The populations of the $|T_{\pm1}\rangle$ sublevels through the |S⟩ → $|T_{\pm1}\rangle$ relaxation may become negligibly small, but these sublevels can be populated through ET of the triplet precursor, ^{3}D*–B–A (Scheme 1a). The observed MFE on $I_{450}(B)$ in a field region of 7.5 mT << B ≤ 1.7 T, which reflects the B-dependence of the decay rate of the $|T_{\pm1}\rangle$ sublevels, can be explained by the RM. The |S⟩ ↔ $|T_0\rangle$ interconversion rate somewhat increases with increasing B owing to the difference in the isotropic g-factors between D$^{•+}$ ($g = 2.0052$[7b]) and A$^{•-}$ ($g = 2.0041$[7b]) (Δg mechanism[18a]). However, this enhancement is not so significant because the magnitude of this interaction (ΔgB) is 1.9 mT under $B = 1.7$ T, which is smaller than $|2J| / g\beta$ and $B_{1/2}$.

(b) Spin Conversion of [D$^{•+}$–B–A$^{•-}$–R•] under Zero Field. The three-spin intermediate, [D$^{•+}$–B–A$^{•-}$–R•], can exist in either of four quartet (|Q⟩) and four doublet (|D⟩, |D′⟩) spin sublevels. In this expression, the |D′⟩ states have the total spin of singlet with respect to D$^{•+}$–A$^{•-}$ pair, while the |D⟩ states have the triplet one.[10f] The energy levels of the |D⟩, |D′⟩ and |Q⟩ states are determined by J(D$^{•+}$, A$^{•-}$), J(D$^{•+}$, R•), and J(A$^{•-}$, R•), where $J(i, j)$ is the exchange interaction between the radical centers, i and j, under zero field.[10] Upon ET of the doublet precursor ^{2}[^{1}D*–B–A–R•], the |D′⟩ states are populated as shown in Scheme 1b. A mono-exponential decay of [D$^{•+}$–B–A$^{•-}$–R•] observed in dioxane (Fig. 2a) can be explained by one of the three cases: Case (i) where all the eight sublevels (|D′⟩, |D⟩, and |Q⟩) are in a thermal equilibrium, Case (ii) where the |D′⟩ and |D⟩ states are equilibrated with no population of the |Q⟩ states, or Case (iii) where only the |D′⟩ states were populated. According to Buchachenko et al., the |D′⟩ ↔ |D⟩ conversion is induced by the difference in the exchange interaction, ΔJ(D$^{•+}$, A$^{•-}$) ≡ |J(D$^{•+}$, R•) – J(A$^{•-}$, R•)|.[10] To obtain experimental evidence for this spin catalysis theory, Turro et al. investigated whether the spin conversion of RPs was affected by the presence of the TEMPO radical, which was introduced in the reaction systems either intermolecularly or intramolecularly (i.e. covalently connected to one of the component radicals of the RPs).[10a,b,e] They observed an enhancement of the

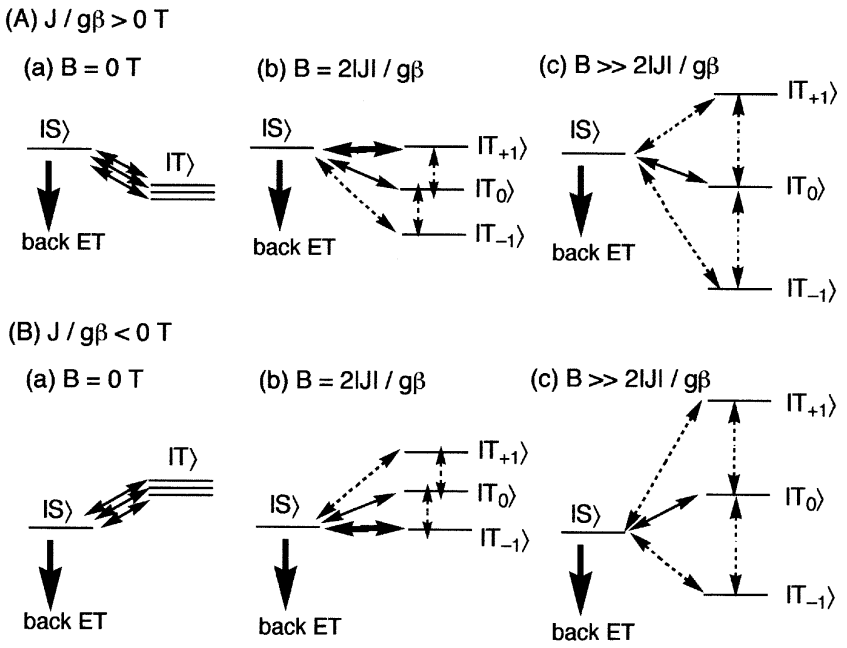

Fig. 6. Energy diagrams and interconversion routes of the spin sublevels for the CS state derived from **2** in the cases of (A) positive J or (B) negative J. The bold (dotted) arrows present processes faster (slower) than those presented by the solid thin arrows.

radical coupling within the RPs by the presence of the TEMPO radical in non-viscous solvents, such as benzene and dioxane, where the lifetimes of the RPs were probably short ($\leq 10^{-9}$ s). In the present case, where $|J(D^{\bullet+}, R\bullet)| << |J(A^{\bullet-}, R\bullet)|$, a large $\Delta J(D^{\bullet+}, A^{\bullet-})$ can cause efficient $|D'\rangle \leftrightarrow |D\rangle$ conversion of $[D^{\bullet+}\text{–B–}A^{\bullet-}\text{–R}\bullet]$ within its lifetime, which is governed by the k_{BET} value (2.74×10^7 s^{-1}). From these facts, it can be considered that thermal equilibrium is established between the $|D'\rangle$ and $|D\rangle$ states during the decay of $[D^{\bullet+}\text{–B–}A^{\bullet-}\text{–R}\bullet]$.

It is expected that information on the $|D\rangle \leftrightarrow |Q\rangle$ conversion process can be obtained from MFEs on the decay dynamics of $[D^{\bullet+}\text{–B–}A^{\bullet-}\text{–R}\bullet]$, because the efficiency of the $|D\rangle \leftrightarrow |Q\rangle$ conversion, but not of the $|D'\rangle \leftrightarrow |D\rangle$ one, is affected by external magnetic fields.[35,36] As shown in Fig. 2, the decay of $[D^{\bullet+}\text{–B–}A^{\bullet-}\text{–R}\bullet]$ at an early time region in dioxane and PenOAc increased with increasing B. The observed MFEs indicate that the $|D\rangle$ states were efficiently converted to the $|Q\rangle$ ones under zero field and that this $|D\rangle \rightarrow |Q\rangle$ conversion was partially inhibited in the presence of B's. The mechanism of the MFEs on $|D\rangle \leftrightarrow |Q\rangle$ conversion is discussed below (in Section 2(c)) in more detail. From the consideration on the $|D'\rangle \leftrightarrow |D\rangle$ and $|D\rangle \leftrightarrow |Q\rangle$ conversion processes, the mono-exponential decay of the $A(t)$ curve observed in dioxane under zero field can be interpreted as first-order decay of an equilibrium mixture of all the eight sublevels, that is Case (i). In such a situation, the observed decay rate corresponds to a quarter of the spin-allowed back ET rate (k_{BET}), because the singlet character with respect to $D^{\bullet+}\text{–}A^{\bullet-}$ pair is one-fourth for each sublevel of $[D^{\bullet+}\text{–B–}A^{\bullet-}\text{–R}\bullet]$.

(c) MFEs on the $|D\rangle \leftrightarrow |Q\rangle$ Conversion of $[D^{\bullet+}\text{–B–}A^{\bullet-}\text{–R}\bullet]$. Previously we studied photo-induced ET reaction of MPTZ with *N*-hexyl-*N*′-(TEMPO-4-yl)-1,2 : 4,5-pyromellitdiimide (PI–R•, see Chart 1) in 2-propanol (2-PrOH).[7b] The observed MFEs on the free-ion yields from the three-spin intermediate, $^{4,2}[MPTZ^{\bullet+}\ PI^{\bullet-}\text{–R}\bullet]$, were explained by the relaxation mechanism for the $|D\rangle \leftrightarrow |Q\rangle$ conversion.[36] We suggested that the $|D\rangle \leftrightarrow |Q\rangle$ conversion of $[MPTZ^{\bullet+}\ PI^{\bullet-}\text{–R}\bullet]$ should be induced by mainly a dipolar interaction between $PI^{\bullet-}$ and R•. The magnitude of this dipolar interaction ($|D_{ZFS}|$) of $PI^{\bullet-}\text{–R}\bullet$ was estimated to be 4.35 mT using a point-dipole approximation with a distance of 8.6 Å between the center of $PI^{\bullet-}$ moiety and the midpoint of the N–O bond in R•.[7b] The observation of large MFEs indicates that this interaction can effectively induce the $|D\rangle \leftrightarrow |Q\rangle$ conversion within the lifetime of the ion-pair in 2-PrOH ($\sim 10^{-8}$ s).

It is likely that the $A^{\bullet-}\text{–R}\bullet$ part in $[D^{\bullet+}\text{–B–}A^{\bullet-}\text{–R}\bullet]$ has almost the same $|D_{ZFS}|$ value as $PI^{\bullet-}\text{–R}\bullet$. Therefore, the MFEs observed for **3** can be explained by the same mechanism as the previous case.[7] Although the estimated $|D_{ZFS}|$ value (4.35 mT) of $[D^{\bullet+}\text{–B–}A^{\bullet-}\text{–R}\bullet]$ is only 1.6-fold of the calculated $B_{1/2}$ value (2.8 mT) of $[D^{\bullet+}\text{–B–}A^{\bullet-}]$, the observed differences in the decay dynamics indicate that the $|D\rangle \leftrightarrow |Q\rangle$ conversion of $[D^{\bullet+}\text{–B–}A^{\bullet-}\text{–R}\bullet]$ should be much faster than the $|S\rangle \leftrightarrow |T\rangle$ conversion of $[D^{\bullet+}\text{–B–}A^{\bullet-}]$ under zero field, as was mentioned above. The $|D\rangle$–$|Q\rangle$ energy gap of $[D^{\bullet+}\text{–B–}A^{\bullet-}\text{–R}\bullet]$ can be either larger or smaller than the $|S\rangle$–$|T\rangle$ gap of $[D^{\bullet+}\text{–B–}A^{\bullet-}]$, depending on the signs and magnitudes of the three J (i, j) values.[10] These J values, however, could not be obtained in the present study because no MFE due to the LCM was observed. The $J(D^{\bullet+}, A^{\bullet-})$ value in $[D^{\bullet+}\text{–B–}A^{\bullet-}\text{–R}\bullet]$ is likely to be similar to that in $[D^{\bullet+}\text{–B–}A^{\bullet-}]$, whereas $|J(D^{\bullet+}, R\bullet)|$ is negligibly small due to the large separation of $D^{\bullet+}$ and R•. Although the $|D\rangle$–$|Q\rangle$ energy gap of $[D^{\bullet+}\text{–B–}A^{\bullet-}\text{–R}\bullet]$ could not be obtained because of the lack of the knowledge on the $J(A^{\bullet-}, R\bullet)$ value,

the occurrence of efficient $|D\rangle \leftrightarrow |Q\rangle$ conversion under zero field suggests that this energy gap may be smaller than the $|S\rangle$–$|T\rangle$ gap of [D•+–B–A•−].

In Fig. 2b, the decay observed at the early time region, which mainly represents the decay of the CS states generated from ^{2}[^{1}D*–B–A–R•], becomes faster with increasing B because the spin conversion to the unreactive $|Q\rangle$ states becomes less efficient. On the other hand, the $A(t)$ curves at the later time region predominantly reflect the decay of the $|Q_{\pm3/2}\rangle$ sublevels. These sublevels may be populated through ET of ^{4}[^{3}D*–B–A–R•]. The decay of the $|Q_{\pm3/2}\rangle$ sublevels is governed by the spin relaxation to $|Q_{\pm1/2}\rangle$ and $|D_{\pm1/2}\rangle$, which becomes slower with increasing B.[36]

A comparison of the photo-induced processes for **3** and **2** demonstrates that the introduction of a nitroxide radical (R•) to the D–B–A system markedly accelerates the spin conversion of the CS states, while the efficiency of the charge separation (Φ_{CS}) and the spin-allowed back ET rate (k_{BET}) were not largely affected by the presence of R•. An enhancement of the spin-conversion rate gives two advantageous features to the photochemical reaction of D–B–A. First, when ET occurs from ^{1}D*, the conversion from the initially generated CS states to the unreactive states with different spin multiplicity decelerates the decay through the back ET. As a result, the CS states can undergo successive reactions other than back ET, such as a charge shift to a secondary donor or acceptor, if available. Secondly, rapid equilibration of all the accessible spin sublevels of the intermediate simplifies its decay kinetics compared with a spin-selective reaction accompanied by slow reversible spin conversion, which is favorable for determining of the reaction rate constants.

3. Solvent Effects on the Decay Dynamics of the CS States. (a) Solvent Effect on k_{BET}. Table 2 shows that the k_{BET} value dramatically increases with increasing solvent polarity. This solvent dependence can be explained as follows. In the limit of the dielectric continuum model, the solvent reorganization energy (λ_{sol}) can be expressed by Eq. 8,[27]

$$\lambda_{sol} = e^2/(8\pi\varepsilon_0)(1/r_D + 1/r_A - 2/R)(1/n^2 - 1/\varepsilon_r), \quad (8)$$

where n is the refractive index of the solvent. As for the internal reorganization energy, we assume that $\lambda_{vib} = 0.3$ eV, which was estimated for an RIP consisting of MPTZ•+ and radical anion of an electron acceptor with one benzene ring in a previous work.[7b] The ΔG_{BET} and λ values estimated by Eqs. 2 and 8, respectively, are listed in Table 2. Approximate ΔG_{BET} values for benzene and dioxane were obtained by subtracting of the reported additional solvation energies (0.4 and 0.55 eV[24]) from ΔG_{BET} calculated for *trans*-decalin by Eq. 2. As the λ_{sol} values for benzene and dioxane, the corresponding values reported by Warman et al. for similar systems were used.[24] Although more accurate ΔG_{BET} and λ values for solvents of low or medium polarity are necessary for a quantitative discussion,[37] Table 2 shows that the back ET reactions vary from a deeply inverted region to the normal region along with an increase in the solvent polarity. The observation that k_{BET} decreases with a decrease in the solvent polarity is consistent with the prediction from Eq. 4. Although the decrease in λ causes an increase in the pre-exponential factor, the decrease in the exponential term is much more dominant. For some other D–B–A compounds, a large solvent dependence of the back ET rate was also reported.[24]

(b) Solvent Effect on J. The solvent effects on the decay dynamics of both [D•+–B–A•−–R•] and [D•+–B–A•−] can be attributed to the solvent dependence of k_{BET}, as discussed above. However, the J(D•+, A•−) value is also affected by the solvent polarity, and the change in J(D•+, A•−) can alter the $|S\rangle \leftrightarrow |T\rangle$ conversion rate of [D•+–B–A•−]. According to the perturbation theory, the exchange interaction can be estimated by[38]

$$J \approx -|V|^2/(\Delta G_{BET} + \lambda). \quad (9)$$

Equation 9 predicts that the J value can vary with solvents through variations in ΔG_{BET} and λ. When $\Delta G_{BET} + \lambda$ is close to zero, this theory cannot be applied, because the right-hand side of Eq. 9 diverges. More rigorous theoretical treatments with an equilibrium distribution for nuclear configurations predict that J becomes zero at $\Delta G_{BET} + \lambda = 0$.[38a,d] As can be seen in Table 2, because $\Delta G_{BET} + \lambda$ for [D•+–B–A•−] in DMSO is nearly zero, the $|S\rangle$ and $|T\rangle$ states are nearly degenerate. In such a case, $|S\rangle \leftrightarrow |T\rangle$ conversion is induced by the HFC interaction with a rate of k_{HFC} ($= 1.2 \times 10^8$ s^{-1} from Eq. 7, vide supra) under zero field. The lack of observation of [D•+–B–A•−] born in the $|S\rangle$ state suggests that k_{BET} in DMSO should be larger than k_{HFC}.

Conclusion

(1) The S_1 state of phenothiazine moiety (^{1}D*) in the present D–B–A(–R•) systems was effectively quenched through the intramolecular ET to give the CS state in high quantum yields, even in solvents of low polarity, such as benzene and toluene. The TEMPO moiety (R•) in **3** also caused excitation energy transfer as another quenching pathway, but the quenching through ET was much faster than the energy transfer. In polar solvents, such as MeCN and DMSO, ET from ^{3}D* to A also occurred to give the CS state with a different spin multiplicity from that formed from ^{1}D*.

(2) The decay dynamics of the CS state was strongly affected by the presence of R•, especially in dioxane. Without R•, most part of ^{1}[D•+–B–A•−] decayed through the spin-allowed back ET, because the conversion to ^{3}[D•+–B–A•−] was much slower due to an exchange interaction larger than $B_{1/2}$. In the presence of R•, $|D\rangle \leftrightarrow |Q\rangle$ conversion was effectively induced by a dipole–dipole interaction between A•− and R•, and the efficient $|D'\rangle \leftrightarrow |D\rangle$ conversion resulted from the difference between J(A•−, R•) and J(D•+, R•). As a result of these fast spin conversions, the decay of the [D•+–B–A•−–R•] born in the $|D'\rangle$ state was markedly retarded compared with [D•+–B–A•−] born in the $|S\rangle$ state. This point is advantageous for efficient chemical transformations initiated by photo-induced ET and/or determination of back ET rates.

(3) The back ET rate constant (k_{BET}) of the CS state to give the ground state varied by more than two orders of magnitude with the solvent property. The k_{BET} value decreased with de-

creasing solvent polarity. This solvent effect can be explained by the fact that the back ET process falls in the deeply inverted region due to the smaller λ_{sol} and the more negative ΔG_{BET} in less-polar solvents.

Experimental

For syntheses, anhydrous THF (stabilizer-free), hexane, toluene, and DMF (Organics, for organic syntheses) were used as received. All of the reactions were carried out under a N_2 atmosphere. Flash chromatography was carried out on silica gel (Kanto Chemicals, Silica gel 60, spherical, 270–325 mesh). IR spectra were obtained as KBr disks. ^{1}H NMR spectra (270 MHz) were measured in CD_2Cl_2 with the signal due to residual ^{1}H of the solvent (δ 5.32) as an internal standard. EPR spectra were recorded at room temperature with 100-kHz modulation on an X-band EPR spectrometer (JEOL, JES-RE1X). The magnetic field and the microwave frequency were determined with an NMR field meter (Echo Electronics, EFM-2000AX) and a microwave counter (Echo Electronics, EMC-14), respectively. A microwave power of 0.8 mW was used. For optical measurements, THF and MeCN were of spectroanalytical grade and dried over Molecular Sieves 3A before use. Benzene and toluene of spectroanalytical grade were used as received. Dioxane was distilled from CaH_2 under a N_2 atmosphere. DMSO of spectroanalytical grade was distilled from CaH_2 under reduced pressure.

10-[(4′-Bromomethylbiphenyl-4-yl)methyl]phenothiazine (6). To a suspension of NaH (5.0 mmol, washed with anhydrous hexane) in THF (6 cm^3), a solution of phenothiazine (0.8 g, 4.0 mmol) in THF was added with stirring. The mixture was stirred under N_2 at room temperature until the evolution of H_2 gas ceased (about 1 h) and at 40 °C for an additional 1 h. The resultant red-brown solution was slowly transferred by a cannula to a 100 cm^3 three-necked flask containing a suspension of 4,4′-bis(bromomethyl)biphenyl (1.70 g, 5.0 mmol) in 30 cm^3 of THF. This mixture was stirred at 60 °C for 3 h, cooled down to room temperature, and filtered. The filtrate was concentrated, diluted with benzene and water. The organic layer was separated, washed with water and then brine, dried over $MgSO_4$, and evaporated. The residue was subjected to flash chromatography with benzene–hexane (1 : 2 to 1 : 1). The obtained bromide **6** was contaminated with a small amount of the starting dibromide, but used for the next step without further purification.

10-[(4′-Aminomethylbiphenyl-4-yl)methyl]phenothiazine (7). A mixture of **6** (500 mg, 1.1 mmol), potassium phthalimide (278 mg, 1.5 mmol) and 18-crown-6 (40 mg, 0.15 mmol) in 10 cm^3 of toluene was stirred at 90 °C for 12 h.[39] The resultant mixture was cooled down to room temperature and diluted with benzene and water. The organic layer was separated, washed with brine, dried over $MgSO_4$, and concentrated. Flash chromatography of the residue eluting with benzene–ethyl acetate (20 : 1 v/v) gave the phthalimide (440 mg). This phthalimide was suspended to EtOH (25 cm^3) and a 6-fold excess of hydrazine monohydrate was added. The resultant mixture was refluxed for 3 h. After cooling, an aqueous solution (10 cm^3) of Na_2CO_3 (320 mg) was added, and concentrated until colorless precipitate was separated. This precipitate was extracted with benzene, and the organic layer was washed with water and brine, dried over $MgSO_4$, and evaporated up to give amine **7** in 58 % yield. IR 3400 (ν_{NH}), 3370 (ν_{NH}), 3050, 2920, 2850, 1591, 1570, 1499, 1485, 1462, 1399, 1371, 1258, 1220, 858, 798, 758, 748 cm^{-1}. ^{1}H NMR δ 3.88 (2H, s, CH_2NH$_2$), 5.13 (2H, s, NCH_2), 6.73 (2H, d, J = 8.0 Hz), 6.89 (2H, t, J = 7.5 Hz), 7.03 (2H, ddd, J = 8.0, 7.5, and 1.3 Hz), 7.11 (2H, dd, J = 7.5 and 1.3 Hz), 7.1–7.4 (4H, m), 7.56 (4H, m).

***N*,*N*′-Bis{[4′-(10-Phenothiazinylmethyl)biphenyl-4-yl]methyl}-1,2:4,5-pyromellitdiimide (2) and *N*-[4′-(10-Phenothiazinylmethyl)biphenyl-4-yl]methyl-*N*′-(2,2,6,6-tetramethylpiperidin-1-oxyl-4-yl)-1,2 : 4,5-pyromellitdiimide (3).** A mixture of **7** (138 mg, 0.35 mmol), 1,2 : 4,5-pyromellitic dianhydride (120 mg, 0.55 mmol), and 4-amino-2,2,6,6-tetramethylpiperidin-1-oxyl(4-amino-TEMPO) (123 mg, 0.72 mmol) in 5 cm^3 of DMF was heated under reflux overnight. The mixture was cooled, poured into water, and extracted with benzene. The organic extracts were washed with water and brine, and concentrated. The residue was subjected to flash chromatography with benzene–ethyl acetate (20 : 1 to 10 : 1 v/v) as the eluent affording **2** and **3** as the first and second fractions, respectively. When **7** and 1,2 : 4,5-pyromellitic dianhydride were reacted in a molar ratio of 2 : 1, **2** was obtained in a higher yield. **2**: IR 3060, 3030, 2930, 2850, 1775 ($\nu_{C=O}$), 1709 ($\nu_{C=O}$), 1593, 1572, 1499, 1464, 1453, 1394, 1260, 1101, 936, 800, 791, 754, 748 cm^{-1}. ^{1}H NMR δ 4.91 (4H, s), 5.12 (4H, s), 6.70 (4H, d, J = 7.5 Hz), 6.87 (4H, td, J = 7.5 and 1.6 Hz), 7.00 (4H, td, J = 7.5 and 1.6 Hz), 7.09 (4H, dd, J = 7.5 and 1.6 Hz), 7.38 (4H, d, J = 8 Hz), 7.5 (8H, AA′BB′), 7.55 (4H, d, J = 8 Hz), 8.26 (2H, s). **3** : IR 3050, 2975, 2938, 1773 ($\nu_{C=O}$), 1713 ($\nu_{C=O}$), 1595, 1572, 1499, 1466, 1442, 1379, 1364, 1342, 1096, 856, 810, 748 cm^{-1}. ^{1}H NMR δ 4.94 (2H, s), 5.13 (2H, s), 6.71 (2H, d, J = 7.8 Hz), 6.88 (2H, t, J = 7.5 Hz), 7.00 (2H, t, J = 7 Hz), 7.10 (2H, d, J = 7 Hz), 7.4 (2H, d, J = 8 Hz), 7.5–7.6 (6H, m), 8.29 (2H, br s).

Attempted Synthesis of *N*-Hexyl-*N*′-[4′-(10-phenothiazinylmethyl)biphenyl-4-yl]methyl-1,2:4,5-pyromellitdiimide (2′). A mixture of **7** (60 mg, 0.15 mmol), 1,2 : 4,5-pyromellitic dianhydride (65 mg, 0.30 mmol), and hexylamine (46 mg, 0.45 mmol) in 3 cm^3 of DMF was heated overnight under reflux. A work-up procedure similar to the case of **2** and **3** gave a mixture of **2′** and *N*,*N*′-dihexyl-1,2 : 4,5-pyromellitdiimide in a ratio of ca. 1 : 1.5 (based on the integration ratio of the ^{1}H NMR signals), which could not be separated from each other after repeated flash chromatography.

***N*-[4′-(10-Phenothiazinylmethyl)biphenyl-4-yl]methyl-*N*′-(2,2,6,6-tetramethylpiperidin-1-oxyl-4-yl)bicyclo[2.2.2]oct-7-ene-2,3 : 5,6-bis(dicarboximide) (4).** A mixture of amine **7** (59 mg, 0.15 mmol), 4-amino-TEMPO (43 mg, 0.25 mmol), and bicyclo[2.2.2]oct-7-ene-2,3:5,6-tetracarboxylic dianhydride (50 mg, 0.20 mmol) in DMF (3 cm^3) was stirred at 130 °C overnight. After cooling to room temperature, the mixture was poured into water and extracted with benzene. The organic extracts were washed with brine, dried over $MgSO_4$, and concentrated. Flash chromatography of the residue with benzene–ethyl acetate (20 : 1 to 4 : 1 v/v) as eluent gave **4** (25 mg, 16%). IR 3060, 3030, 2970, 2930, 1773 ($\nu_{C=O}$), 1701 ($\nu_{C=O}$), 1595, 1575, 1500, 1464, 1443, 1377, 1255, 1213, 804, 781, 752 cm^{-1}. ^{1}H NMR δ 2.91 (2H, br s), 3.02 (2H, s), 3.72 (2H, br s), 4.58 (2H, s, imide–CH_2), 5.13 (2H, s, phenothiazine–CH_2), 6.04 (2H, br s, olefinic H), 6.71 (2H, d, J = 7.3 Hz), 6.88 (2H, t, J = 7.3 Hz), 7.01 (2H, t, J = 7.3 Hz), 7.10 (2H, d, J = 7.3 Hz), 7.31 (2H, d, J = 7.6 Hz), 7.39 (2H, d, J = 7.6 Hz), 7.52 (2H, d, J = 7.6 Hz), 7.54 (2H, d, J = 7.6 Hz).

***N*-(Biphenyl-4-yl)-*N*′-(2,2,6,6-tetramethylpiperidin-1-oxyl-4-yl)-1,2:4,5- pyromellitdiimide (5).** A mixture of 4-phenylbenzylamine (366 mg, 2.0 mmol), 4-amino-TEMPO (1.0 g, 5.8 mmol), and 1,2 : 4,5-pyromellitic dianhydride (763 mg, 3.5 mmol) in DMF (14 cm^3) was heated under reflux overnight. After cooling

to room temperature, the reaction mixture was poured into water, and the precipitate was collected by filtration, washed with water, and dried in air. The filtrate was extracted with CH_2Cl_2 and the organic extracts were washed with 1 M (1 M = 1 mol dm^{-3}) HCl, water and then brine, dried over $MgSO_4$, and evaporated. The resultant residue and the collected precipitate were combined and purified by flash chromatography with CH_2Cl_2–ethyl acetate as eluent. The first orange-colored band gave the desired product **5** (272 mg).

10-[(Biphenyl-4-yl)methyl]phenothiazine (1) was prepared from phenothiazine and 4-bromomethylbiphenyl by the same procedures as those for **6**. IR 3057, 2851, 1590, 1568, 1487, 1460, 1453, 1408, 1373, 1327, 1284, 1255, 856, 828, 754, 731, 692 cm^{-1}. ^{1}H NMR δ 5.14 (2H, s), 6.73 (2H, d, J = 8 Hz), 6.88 (2H, m), 7.02 (2H, td, J = 7.3 and 1.7 Hz), 7.10 (2H, dd, J = 7.3 and 1.7 Hz), 7.30–7.45 (5H, m), 7.55–7.61 (4H, m).

Electrochemistry. Cyclic voltammograms of **1** and **5** were recorded with a BAS CV-1B voltammetric controller in MeCN containing 0.1 M n-Bu_4NBF_4 as the supporting electrolyte under Ar at ca. 298 K. Glassy carbon, Pt wire, and Ag/Ag$^+$ (BAS RE-5) were used as the working, counter, and reference electrodes, respectively. The scan rate was 50 mV s^{-1}. The ferrocene was used as the internal standard, which showed a reversible redox wave (the peak separation was 60 mV between the cathodic and anodic scans) at –0.365 V vs. SCE in our electrolytic solutions.

Fluorescence Spectra. Fluorescence spectra were recorded on a Shimadzu RF510 spectrofluorometer equipped with a quantum counter at 293 K. Each of the sample solutions (ca. 5 cm^3) in a long-necked quartz cell (10 × 10 × 45 mm) was bubbled with Ar for 20 min before the measurements. The relative quantum yields of fluorescence were determined based on the integrated intensity after subtracting of the background due to the Raman scattering by the solvent.

Laser Flash Photolyses. All measurements were carried out at 293 K. Each of the sample solutions (ca. 2.5 cm^3) was placed in a long-necked quartz cell (10 × 5 × 45 mm) and bubbled with Ar for 20 min before the measurements. The magnetic fields were generated by a Tokin SEE-10W electromagnet. The third (355 nm) harmonic of a Quanta-Ray GCR-103 Nd : YAG laser was used as excitation light. The monitored wavelength of the $A(t)$ curves was chosen for each sample solution so that the maximal absorbance change (A_{max}) on excitation was in a range of 0.12–0.22 (transmittance of 60–75% relative to that before excitation). The concentration of **3** was (1–2) × 10^{-4} M, while for **2** saturated solutions were used (≤ 1 × 10^{-4} M). The optical densities at 355 nm were 0.12–0.13 and 0.7–0.12 for **3** and **2**, respectively, with a path length of 1 cm.

YM thanks the financial supports from The Nishida Research Fund for Fundamental Organic Chemistry and from Kenkyu-Shoureihi (Research Facilitation Grant) of RIKEN.

References

1 M. R. Wasielewski, *Chem. Rev.*, **92**, 435 (1992).

2 D. Gust, T. A. Moore, and A. L. Moore, *Acc. Chem. Res.*, **26**, 198 (1993).

3 a) C. Luo, D. M. Guldi, H. Imahori, K. Tamaki, and Y. Sakata, *J. Am. Chem. Soc.*, **122**, 6535 (2000). b) H. Tsue, H. Imahori, T. Kaneda, Y. Tanaka, T. Okada, K. Tamaki, and Y. Sakata, *J. Am. Chem. Soc.*, **122**, 2279 (2000), and references therein.

4 "Electron Transfer : from Isolated Molecules to Biomolecules. Part I and II," ed by M. Bixon and J. Jortner, Wiley, New York (1999).

5 a) For example, R. J. Hulsebosch, I. V. Borovykh, S. V. Paschenko, P. Gast, and A. J. Hoff, *J. Phys. Chem. B*, **103**, 6815 (1999). b) Recent review, K. Möbius, *Chem. Soc. Rev.*, **2000**, 129.

6 a) D. Carbonera, M. D. Valentin, C. Corvaja, G. Agostini, G. Giacometti, P. A. Liddell, D. Kuciauskas, A. L. Moore, T. A. Moore, and D. Gust, *J. Am. Chem. Soc.*, **120**, 4398 (1998). b) G. Elger, H. Kurreck, A. Wiehe, E. Johnen, M. Fuhs, T. Prisner, and J. Vrieze, *Acta Chem. Scand.*, **51**, 593 (1997). c) F. Lendzian, J. Schlüpmann, J. von Gersdorff, K. Möbius, and H. Kurreck, *Angew. Chem., Int. Ed. Engl.*, **39**, 1461 (1991).

7 a) Y. Mori, Y. Sakaguchi, and H. Hayashi, *Chem. Phys. Lett.*, **286**, 446 (1998). b) Y. Mori, Y. Sakaguchi, and H. Hayashi, *J. Phys. Chem. A*, **104**, 4896 (2000).

8 Y. Mori, Y. Sakaguchi, and H. Hayashi, *Chem. Phys. Lett.*, **301**, 365 (1999).

9 a) A. J. Hoff and P. J. Hore, *Chem. Phys. Lett.*, **108**, 104 (1984). b) K. M. Salikhov, A. J. van der Est, and D. Stehlik, *Appl. Magn. Reson.*, **16**, 101 (1999).

10 a) E. N. Step, A. L. Buchachenko, and N. J. Turro, *J. Am. Chem. Soc.*, **116**, 5462 (1994). b) A. L. Buchachenko, L. V. Ruban, E. N. Step, and N. J. Turro, *Chem. Phys. Lett.*, **233**, 315 (1995). c) A. L. Buchachenko and V. L. Berdinsky, *Russ. Chem. Bull.*, **44**, 1578 (1995); Translated from *Izv. Akad. Nauk. Ser. Khim.*, **1995**, 1646. d) A. L. Buchachenko and V. L. Berdinsky, *J. Phys. Chem.*, **100**, 18292 (1996). e) A. L. Buchachenko, V. L. Berdinsky, and N. J. Turro, *Kinetics and Catalysis*, **39**, 301 (1998); Translated from *Kinetika i Kataliz*, **39**, 325 (1998). f) A. L. Buchachenko and V. L. Berdinsky, *Chem. Phys. Lett.*, **298**, 279 (1998). In our case, the $|D\rangle$ and $|D'\rangle$ states in the presence of magnetic fields should be expressed as follows instead of Eqs. (2g) and (2h) in their paper: $|D_{+1/2}\rangle = 6^{-1/2}(2|\alpha_{D\bullet}+\alpha_{A\bullet}-\beta_{R\bullet}\rangle - |\alpha_{D\bullet}+\beta_{A\bullet}-\alpha_{R\bullet}\rangle - |\beta_{D\bullet}+\alpha_{A\bullet}-\alpha_{R\bullet}\rangle)$; $|D_{-1/2}\rangle = 6^{-1/2}(2|\beta_{D\bullet}+\beta_{A\bullet}-\alpha_{R\bullet}\rangle - |\beta_{D\bullet}+\alpha_{A\bullet}-\beta_{R\bullet}\rangle - |\alpha_{D\bullet}+\beta_{A\bullet}-\beta_{R\bullet}\rangle)$; $|D'_{+1/2}\rangle = 2^{-1/2}(|\alpha_{D\bullet}+\beta_{A\bullet}-\alpha_{R\bullet}\rangle - |\beta_{D\bullet}+\alpha_{A\bullet}-\alpha_{R\bullet}\rangle)$; $|D'_{-1/2}\rangle = 2^{-1/2}(|\alpha_{D\bullet}+\beta_{A\bullet}-\beta_{R\bullet}\rangle - |\beta_{D\bullet}+\alpha_{A\bullet}-\beta_{R\bullet}\rangle)$.

11 A. I. Ivavov, V. A. Mikhailova, and S. V. Feskov, *Appl. Magn. Reson.*, **16**, 481 (1999).

12 Y. Moroi, A. M. Braun, and M. Grätzel, *J. Am. Chem. Soc.*, **101**, 567 (1979).

13 Y. Sakaguchi and H. Hayashi, *J. Phys. Chem. A*, **101**, 549 (1997).

14 a) M. Kaholek and P. Hrdlovic, *J. Photochem. Photobiol. A: Chem.*, **127**, 45 (1999). b) N. V. Blough and D. J. Simpson, *J. Am. Chem. Soc.*, **110**, 1915 (1988). c) S. A. Green, D. J. Simpson, G. Zhou, P. S. Ho, and N. V. Blough, *J. Am. Chem. Soc.*, **112**, 7337 (1990). d) S. E. Herbelin and N. V. Blough, *J. Phys. Chem. B*, **102**, 8170 (1998).

15 The D–R• distance in **4** is somewhat different from that in **3**, because the bicyclic diimide part in **4** is not planar as the 1,2 : 4,5-pyromellitdiimide part in **3**. However, we could not obtain any better D–B–R• model compound than **4**.

16 U. Werner, Y. Sakaguchi, H. Hayashi, G. Nohya, R. Yoneshima, S. Nakajima, and A. Osuka, *J. Phys. Chem.*, **99**, 13930 (1995).

17 Y. Fujiwara, R. Nakagaki, and Y. Tanimoto, "Dynamic Spin Chemistry," ed by S. Nagakura, H. Hayashi, and T. Azumi, Kodansha–Wiley, Tokyo and New York (1998), Chap. 3.

18 a) H. Hayashi, "Dynamic Spin Chemistry," ed by S. Nagakura, H. Hayashi, and T. Azumi, Kodansha–Wiley, Tokyo and New York (1998), Chap. 2. b) H. Hayashi and S. Nagakura, *Bull. Chem. Soc. Jpn.*, **51**, 2862 (1978).

19 In MeCN and DMSO, the $A(t)$ curves did not decay to the zero level within 1 μs, but a small fraction of non-decaying component (ca. 5% of A_{max}) was observed. This component probably corresponded to the absorption due to the singly charged ions which were formed by the following intermolecular charge shift reaction.

$$D^{\bullet+}\text{–}B\text{–}A^{\bullet-}\text{–}R\bullet + D\text{–}B\text{–}A\text{–}R\bullet \rightarrow D\text{–}B\text{–}A^{\bullet-}\text{–}R\bullet + D^{+\bullet}\text{–}B\text{–}A\text{–}R\bullet$$

20 A. Z. Weller, *Z. Phys. Chem.*, **1982**, 133.

21 J. J. P. Stewart, *J. Comp. Chem.*, **10**, 209 and 221 (1989).

22 a) The structure optimization was carried out for **2′** by the PM3 methods with the program package MOPAC.[22b] Two stable conformers with almost the same energy were obtained , and their R values were 12 and 14 Å. For the CS state, the shorter value was used, because the larger Coulombic stabilization was obtained. b) WinMOPAC Ver. 2.0, Fujitsu Ltd., Japan, 1997.

23 Y. Kawanishi, N. Kitamura, and S. Tazuke, *J. Phys. Chem.*, **90**, 2469 (1986).

24 a) J. M. Warman, M. P. de Haas, J. W. Verhoeven, and M. N. Paddon-Row, in Ref. 4, pp. 571–601. b) J. M. Warman, K. J. Smit, M. P. de Haas, S. A. Jonker, M. N. Paddon-Row, A. M. Oliver, J. Kroon, H. Oevering, and J. W. Verhoeven, *J. Phys. Chem.*, **95**, 1979 (1991).

25 M. J. Shephard and M. N. Paddon-Row, *J. Phys. Chem. A*, **103**, 3347 (1999).

26 S. Nath, H. Pal, D. K. Palit, A. V. Sapre, and J. P. Mittal, *J. Phys. Chem. A*, **102**, 5822 (1998).

27 R. A. Marcus, *J. Chem. Phys.*, **24**, 966 and 979 (1956).

28 The magnitude of V largely depends on the ET mechanism. In some D–B–A systems, two-step sequential ET involving an intermediate in which the bridge part bears a charge (D^+–B^-–A or D–B^+–A^-) has been postulated.[29] In the present case, however, the sequential mechanism involving $D^{\bullet+}$–$B^{\bullet-}$–A can be ruled out, because no charge separation occurred in **1** even in solvents of high polarity such as MeCN. The ΔG_{ET} value for the hypothetical ET reaction of $^1D^*$–B to give $D^{\bullet+}$–$B^{\bullet-}$ was estimated to be ca. +0.2 eV from Eq. 2, with E_{RED} of biphenyls (–2.36 and –2.55 V vs. SCE for unsubstituted and 4,4′-di-*t*-butyl substituted compounds),[30] E_{OX} of **1** (+ 0.71 V vs. SCE), $R \approx 6$ Å, and $E_S = 2.9$ eV. Thus, this hypothetical ET is energetically unfavorable. It is likely that the single-step long-distance ET from $^1D^*$ to A takes place by the super-exchange mechanism.[31]

29 a) R. A. Marcus, *Chem. Phys. Lett.*, **133**, 471 (1987). b) S. F. Fischer and P. O. J. Scherer, *Chem. Phys.*, **115**, 151 (1987). c) M. -E. Michel-Beyerle, M. Bixon, and J. Jortner, *Chem. Phys. Lett.*, **151**, 188 (1988). d) M. Volk, G. Aumeier, T. Langerbacher, R. Feick, A. Ogrodnik, and M. -E. Michel-Beyerle, *J. Phys. Chem. B*, **102**, 735 (1998).

30 a) P. K. Freeman and L. L. Hutchinson, *J. Org. Chem.*, **45**, 1924 (1980). b) M. D. Curtis and A. L. Allred, *J. Am. Chem. Soc.*, **87**, 2554 (1965). c) In Ref. 30a, the reduction potential of naphthalene in DMF was reported to be –1.98 V vs. mercury pool. If the redox potentials are the same in DMF and MeCN, this value corresponds to –2.29 V vs. SCE.[30d] d) G. J. Kavarnos and N. J. Turro, *Chem. Rev.*, **86**, 401 (1986).

31 a) M. Bixon and J. Jortner, in Ref. 4, pp. 35–202. b) H. M. McConnel, *J. Chem. Phys.*, **35**, 508 (1961).

32 The decay rate of the T_1 state of MPTZ (1.5×10^5 s^{-1} in 2-PrOH at 293 K under N_2 atmosphere) determined at a higher concentration (1×10^{-3} M).[7b]

33 a) G. -H. Goudsmit, H. Paul, and A. I. Shushin, *J. Phys. Chem.*, **97**, 13243 (1993). b) A. I. Shushin, *Z. Phys. Chem.*, **182**, 9 (1993). c) A. I. Shushin, *Chem. Phys. Lett.*, **208**, 173 (1993). d) A. Kawai, T. Okutsu, and K. Obi, *J. Phys. Chem.*, **95**, 9130 (1991). e) A. Kawai and K. Obi, *J. Phys. Chem.*, **96**, 5701 (1992). f) Y. Kobori, K. Takeda, K. Tsuji, A. Kawai, and K. Obi, *J. Phys. Chem. A*, **102**, 5160 (1998).

34 (a) A. Weller, K. Nolting, and H. Staerk, *Chem. Phys. Lett.*, **96**, 24 (1983). b) K. Schulten and P. G. J. Wolynes, *Chem. Phys.*, **68**, 3292 (1978).

35 a) L. R. Faulkner, H. Tachikawa, and A. J. Bard, *J. Am. Chem. Soc.*, **94**, 691 (1972). b) H. Tachikawa and A. J. Bard, *Chem. Phys. Lett.*, **26**, 10 and 246 (1974). c) K. Razi Naqvi, H. Staerk, and T. Gillbro, *Chem. Phys. Lett.*, **49**, 160 (1977). d) Y. Iwasaki, K. Maeda, and H. Murai, The Sixth International Symposium on Magnetic Field and Spin Effects in Chemistry and Related Phenomena, Emmetten, Switzerland, Book of Abstracts, p. 67 (1999).

36 a) R. C. Johnson and R. E. Merrifield, *Phys. Rev. B*, **1**, 896 (1970). b) D. R. Kearns and A. J. Stone, *J. Chem. Phys.*, **55**, 3383 (1971). c) P. W. Atkins and G. T. Evans, *Mol. Phys.*, **29**, 921 (1975). d) K. Schulten, *J. Chem. Phys.*, **80**, 3668 (1984).

37 Photoexcitation of some D–B–A systems to a charge-separated excited state in benzene and dioxane required excess reorganization energies of 0.4 and 0.55 eV, respectively, compared with the same process in *trans*-decalin.[24] PenOAc has a relatively low macroscopic dielectric constant, but contains an ester group, which could have strong interactions with charged solutes.

38 a) Y. Kobori, K. Akiyama, and S. Tero–Kubota, *J. Chem. Phys.*, **113**, 465 (2000). b) Y. Kobori, S. Sekiguchi, K. Akiyama, and S. Tero–Kubota, *J. Phys. Chem. A*, **103**, 5416 (1999). c) S. Sekiguchi, Y. Kobori, K. Akiyama, and S. Tero–Kubota, *J. Am. Chem. Soc.*, **120**, 1325 (1998). d) M. Volk, T. Häberle, R. Feick, A. Ogrodnik, and M.-E. Michel-Beyerle, *J. Phys. Chem.*, **97**, 9831 (1993). e) M. Y. Okamura, R. A. Isaacson, and G. Feher, *Biochim. Biophys. Acta*, **546**, 394 (1979).

39 Advantage of addition of a catalytic amount of crown ether was reported. K. Soai, A. Ookawa, and K. Kato, *Bull. Chem. Soc. Jpn.*, **55**, 1671 (1982).

40 "Handbook of Chemistry and Physics," 77th edition, ed by D. R. Lide, CRC Press, FL (1996), pp. 6–151.